Corrosion behavior of different Al_2O_3-MgO-C bricks tested in dynamic conditions

W. A. Calvo¹, M. L. Dignani², S. Camelli², A. G. Tomba Martinez¹*

¹Instituto de Investigaciones en Ciencia y Tecnología de Materiales (INTEMA),
CONICET-Universidad Nacional de Mar del Plata, Av. Colón 10850 (7600) Mar del Plata, Argentina.
²Instituto Argentino de Siderurgia (IAS), Av. Central and Calle 19, Oeste (2900) San Nicolás de los Arroyos, Argentina.

Abstract

The slag corrosion of Al_2O_3-MgO-C refractories for steelmaking ladles is addressed by a dynamic test by considering their characteristics, the experimental approach, and previous cup test data and thermodynamic simulation. To obtain reliable results, an alternative to the current practice of using the samples' dimensions to estimate the corrosion wear was proposed. The brick with the higher periclase content and high open porosity was less resistant in the dynamic test. However, in the other two bricks, the smaller particles and the lower corrosion resistance of bauxite were considered the determining factors for the greater increase in wear during the dynamic test concerning the cup test.

Keywords: Al_2O_3-MgO-C refractories, steelmaking ladle, slag corrosion, laboratory testing.

INTRODUCTION

Al_2O_3-MgO-C (AMC) refractories are widely used in the steelmaking industry for the metal line and the bottom of ladles' lining; in certain steps of the secondary metallurgy process, AMC bricks are in contact with the liquid slag [1]. This research is part of a wider study on the slag corrosion behavior of Al_2O_3-MgO-C (AMC) bricks—a member of the oxide-carbon refractories used extensively in the steelmaking industry but less popular than MgO-C products—which also focuses on testing aspects. Within this framework, different types of AMC refractories were experimentally evaluated in the lab using conventional static (cup test) and dynamic (rotary dipping test) methodologies, and the obtained results have been carefully analyzed considering the testing conditions and the materials' characteristics [1-4]. Comparatively studying different types of refractories has contributed to understanding the distinctive aspects of each laboratory test, and *vice versa*. This is critical to relating the experimental results to the industrial conditions and correctly interpreting them, especially when they will be used for material selection purposes. An example of the usefulness of well-interpreted laboratory data to understand the in-service degradation of AMC bricks has been also reported by the authors [3, 5].

One of the many problems we faced when focusing our analysis on a specific compositional variable of AMC refractories was the inability to maintain some of the bricks' critical characteristics unchanged [1, 2, 6]; for instance, porosity is unquestionably affected by the amount and granulometry of any of the material's components. For this reason, a careful in-depth analysis of the complete system is required, including the analysis of several corrosion indicators, not just the wear or slag penetration currently obtained from conventional tests.

The rotary dipping (or finger) test is a simple way to evaluate the refractories' corrosion behavior in the laboratory since it comes closer to recreating industrial conditions than the static tests (hot microscopy and cup test). According to the review of Reynaert *et al.* [7] and compared with other corrosion tests currently used to evaluate refractory materials, the rotary dipping test is a medium-scaled test that is easy to perform with a large volume of slag concerning the sample size (which avoids slag saturation). It also allows for good temperature control and the possibility of changing the atmosphere. Other dynamic alternatives such as the induction furnace test and the rotary slag test cannot be carried out on a laboratory scale since they are more expensive and are difficult to perform. It is also hard to control some of the experimental conditions such as temperature, atmosphere, etc. [7, 8].

In the dipping test, either static or dynamic, a refractory bar is heated separately from the slag melted in a crucible, and when the target temperature is reached, the sample is submerged in the liquid for a certain period; the atmosphere can be controlled if the furnace is heated in a chamber. The rotation speed can be varied to control the degree of interaction between the refractory bar and the slag, and it can be also renewed to avoid liquid saturation. The dipping test simulates better than the cup test the corrosion conditions that exist in the industry: a) the refractory lining is heated without contact with the slag, b) there is a relative movement between the liquid slag and the refractory, and c) the presence of electromagnetic fields [9]. For this reason, the extrapolation of in-lab results to actual practices is less limited for the dipping test than for the static test.

This work aims to evaluate AMC bricks—which differ from each other mainly in the amount and particle size of the periclase and the source of alumina particles—using the dynamic conditions inherent in a rotary dipping test. As the main contributions, the analysis includes the effect of the materials' characteristics and critical aspects of the experimental approach which the authors have not found discussed in any previous literature. The corrosion behavior of the same AMC bricks under static conditions, and the data obtained from the thermodynamic simulation of the slag-refractory interaction [2, 3, 5], are also considered in the analysis.

MATERIALS AND METHODS

Two commercial AMC refractory bricks manufactured by the same supplier for steelmaking use, labeled as AMC2 and AMC3, are tested using a dynamic slag corrosion test. Their behavior is compared with a third AMC brick previously tested under the same conditions [3], labeled AMC4. The bricks have different magnesia contents and particle sizes as well as different raw materials as the source of alumina. The main characteristics of the refractories are summarised in Table I [10, 11].

The corrosion tests were carried out using an industrial basic slag [1], which has the chemical composition shown in Table II, a ternary basicity ($CaO/(SiO_2+Al_2O_3)$, in mass) of 1.5, and a softening temperature of $1366 \pm 5°C$.

The rotary dipping test was carried out at 1600°C using a 2x2x20 cm^3 rod extracted from the as-received brick. The slag (200 g) was placed inside a graphite crucible (covered with Mo foil), over which the refractory rod was held vertically. The slag-sample ensemble was heated in a lab-made induction furnace to 1600°C (the heating program

lasted ~2 hours); the sample was protected from the air by a glass container. Then, 3 centimeters of the refractory rod were immersed in the melt; the bar was also rotated at 25 rpm. The contact between the refractory sample and the liquid slag was maintained for 30 min; after this time, the sample was pulled out of the melt and allowed to cool outside the furnace. After the test, the corroded rod was cut and prepared for further analysis, including SEM, as was previously described [3].

The wear of the rods after the dipping test was obtained using the following equation:

$$wear = \frac{\text{initial size - final-size}}{\text{initial size}} .100 \qquad (A)$$

The rod thickness at the beginning and the end of the test (*initial size* and *final size* in eq. (1), respectively) is commonly used for the calculation [7]. However, which dimensions have to be considered for a reliable value of the corrosion wear will be further discussed.

RESULTS

The aspect of the corroded bars of AMC2 (shown as an example in Figure 1) and AMC3 were like that for AMC4 [3].

The current practice to determine corrosion wear is based on the dimensional change of the bars after the test using equation (1). The *size* corresponds to the bar's thickness along any (or both) of the cross-section dimensions, determined before (*initial*) and after (*final*) the test [7]. The measurements can be made at different distances from the inferior bar end which was submerged into the liquid slag. Considering that the sample tends to lose material (by detachment or dissolution of particles) during the rotary dipping test, the wear value would be positive. Table III

Table I. Characteristics of AMC bricks.

		AMC2	AMC3	AMC4
Main phases (wt. %)	Corundum (Al_2O_3)	57.6±0.3	76.6±0.3	77.7±0.5
	Periclase (MgO)	27.0±0.1	6.80±0.03	6.6±0.1
	Graphite (C)	3.5±0.1	3.0±0.1	1.9±0.1
Secondary phases (wt. %)	Resin (C. O. H)	5.6±0.1	5.0±0.1	4.4±0.1
	Aluminium (Al)	1.37±0.02	1.60±0.02	2.8±0.1
	Silicon (Si)	0	0	0.35±0.05
Impurities (wt. %)	Fe_2O_3, SiO_2, CaO, TiO_2[1]	4.93±0.05	6.97±0.05	6.25±0.05
Apparent porosity (%)		7.8±0.5	4.0±0.1	3.6±0.1
Decarburized area [1400°C] (%)		100	73	57
Permanent linear change[1400°C] (%)		1.66	0.25	1.34

[1] *Impurities expressed as oxides.*

Table II. Chemical composition of the slag.

Composition (wt.%)							
CaO	Al_2O_3	MgO	SiO_2	FeO	S	Cr_2O_3	MnO
54.90	30.80	8.20	5.00	0.37	0.52	0.01	0.12

shows the wear values determined using the rod's thickness before and after the test at ~ 2.5 cm from the submerged end of the sample. According to these values, AMC2 exhibits negative wear, indicating an increase in the bar dimensions, which is incompatible with what the parameter attempts to measure. At first sight, this result may be partially attributed to the slag adhering to the sample surface (Figure 1), which counterbalances the material loss.
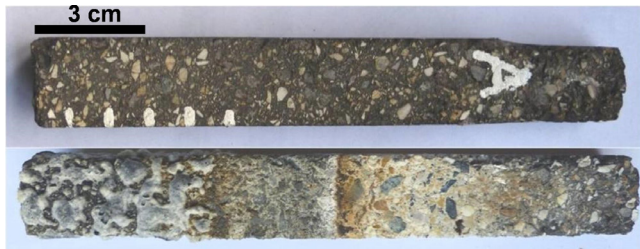

Figure 1. AMC2 rods before (top) and after (bottom) the rotary dipping test (1600°C).

To find another way to make a suitable measurement of corrosion wear, a second method was considered which involves measuring the area of the cross-section as follows: a) the *initial area* was calculated with the dimensions measured before the dipping test at ~2.5 cm from the submerged end of the sample and b) the *final area* was determined by image analysis (ImageJ software) of a photograph of the cross-section obtained by cutting the sample at ~2.5 cm from the end, discounting the slag adhered to the external surface. To do this, (manually) locating the boundary between the refractory and the remnant slag is required (Figure 2); obviously, this process possesses some uncertainty since it relies on the operator's criteria.

The corrosion wear estimated for the AMC bricks using the second method is shown in Table III and is ≥ 0 in every case. These values were considered more reliable and, they are generally in line with the refractories' characteristics and their corrosion behavior as determined by the static tests and the thermodynamic simulation [1-4]. Data from these two analyses are shown in Table III and represent the wear determined in the cup test at 1600°C and the number of iterations (or calculation steps—CS) needed to reach the corrosion end in the thermodynamic simulation (considered as an indicator of the slag corrosion wear [2]). For these reasons, the wear obtained using the cross-section area as described above was used in the further analysis of the AMC bricks' corrosion behavior.
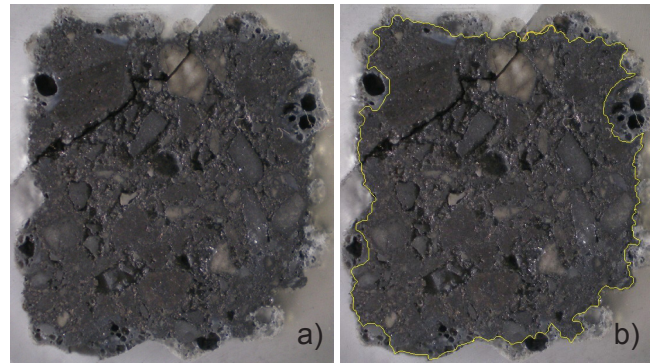

Figure 2. Cross section of the AMC2 bar after the rotary dipping test (left) and the boundary drawn in yellow between the remnant slag and the refractory (right).

SEM images of the refractory/slag interface after the dipping test of AMC2 and AMC3 at 1600ºC are shown in Figure 3. Severe damage was observed in both cases, with highly corroded aggregates and degraded matrix, along with the infiltration of slag through the particles' grain boundaries, like that observed in the previously analyzed material AMC4 [3]. The attacked region in AMC2 is more extensive than in AMC3, with deeper slag penetration. Furthermore, the last refractory was even less infiltrated by the slag than was AMC4. Erosion due to the dragging of intermediate-size particles is observed in the corroded areas of AMC2 and AMC3.

Overall, the new phases formed by the slag attack on AMC2 and AMC3 were the same as those identified under static conditions (cup test [2]) and for the AMC4 sample tested by dipping [3], which confirms that the corrosion mechanism didn't change in either case for these two AMC refractories.

Brown fused alumina aggregates were identified in the slag/refractory interface for AMC2 and AMC3 (Figure 3). Degraded aggregates of tabular alumina were also detected, but only for AMC2 (Figure 3). In the dipping test, the refractory sample and the molten slag come in contact after the target temperature is reached. For this reason, the liquid slag can more easily penetrate and dissolve the refractory components and, therefore, the attack on the matrix and the coarser aggregates can be produced almost simultaneously. Conversely, the finer and more reactive particles are attacked first in the cup test.

The high wear exhibited by other alumina particles

Table III. Slag corrosion parameters.

Corrosion conditions	Parameter	AMC2	AMC3	AMC4
Dynamic	Wear by length (%)	-3.8	2.3	2.3
	Wear by area (%)	28	19	17
Static	Wear in cup test (%)	20	10	6
	CSf [(1)]	~100	4	3

[(1)]*CSf corresponds to the calculation step (CS) number to reach the thermodynamic equilibrium in the simulation of the slag-refractory interaction [2, 3].*
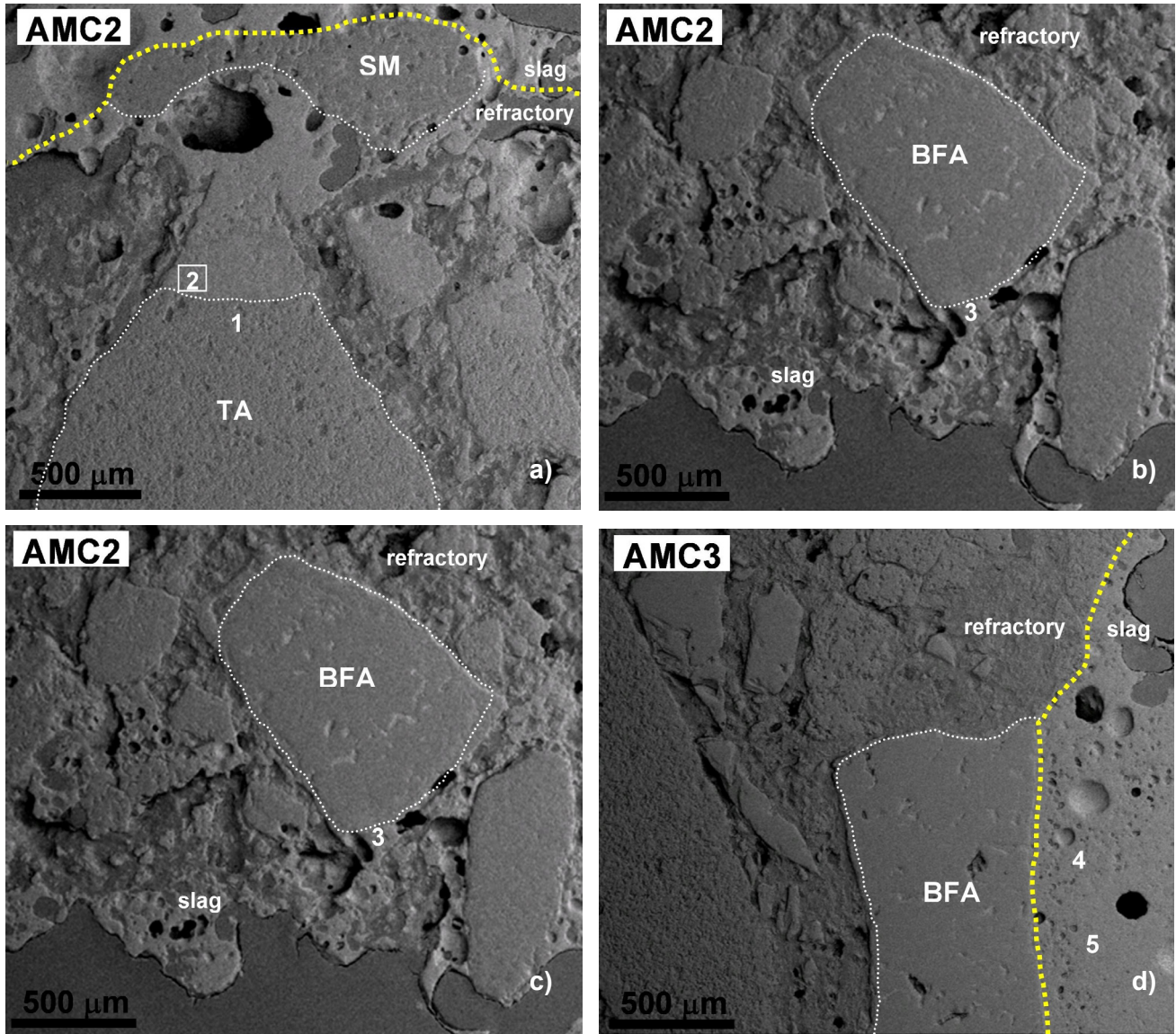
Figure 3. SEM images of the refractory/slag interface after the rotary dipping test and phases proposed for EDS points (the dashed line indicates approximately the refractory/slag interface and the particles boundaries; TA: tabular alumina; BFA: brown fused alumina; Bx: bauxite; SM: sintered magnesia). Phases (EDS point) Al2O3+MA (1), CA2+CA+MA+C-A-S (2), CA+CA2 (3), MA+CA+CA2 (4), MA+CA+CA2+C-A-S (5).

prevents categorical identification in both AMC materials; in the case of AMC3, tabular alumina could not be distinguished. Partially attacked magnesia particles were not identified in the reaction zone in AMC3 either due to the small size of this component. These particles were only detected in AMC2, where they were strongly attacked (Figure 4).

MgAl$_2$O$_4$ spinel (MA), calcium hexaluminate (CaAl$_{12}$O$_{19}$, CA$_6$), and calcium dialuminate (CaAl$_4$O$_7$, CA$_2$) were found as the main formed phases surrounding the alumina particles in AMC2. No layers or clusters were observed for any of these new phases; conversely, these solids were mixed among them. Moreover, compositions with other aluminates such as celite (Ca$_3$Al$_2$O$_6$, C$_3$A)/mayenite (Ca$_{12}$Al$_{14}$O$_{33}$, C$_{12}$A$_7$) and calcium monoaluminate (CaAl$_2$O$_4$, CA) together with MA were

proposed for the bulk of the slag in the vicinity of such particles. In addition, the presence of silicon-containing ternary phases such as gehlenite (Ca$_2$Al$_2$SiO$_7$, C$_2$AS) and/ or anorthite (CaAl$_2$Si$_2$O$_8$, CAS$_2$) were identified. The EDS analyses of corroded periclase particles determined the presence of MA, C$_3$A/C$_{12}$A$_7$, CA, and phases containing CaO, Al$_2$O$_3$, and SiO$_2$ (C-A-S) in their vicinity. The strong damage undergone by these particles did not allow the identification of "internal slag" [2, 3, 12].

The same new phases were proposed in the vicinity of the alumina particles identified in the worn region of AMC3, which were also observed mixed among them. However, compositions compatible with the presence of CA$_6$ were not detected alongside the particles but within them, which occurred for this refractory when tested under static corrosion conditions [2].

DISCUSSION

According to the above dipping test results, the ranking of the three refractories was the same as obtained using the cup test at the same temperature (1600°C). In terms of slag corrosion resistance, the ranking is: AMC2 << AMC3 < AMC4. Based on just the thermodynamic simulation of the slag-AMC interaction, the lower corrosion resistance of AMC2, evidenced by the higher amount of calculation steps (CS) to reach the condition for corrosion stop (CSf in Table III), can be justified by the high magnesia content together with the amount of liquid present in the equilibrium condition (> 60 wt.% for AMC2 and null for AMC3 and AMC4) and the viscosity of this liquid phase (3.0 mPa.s for AMC2, 4.4 mPa.s for AMC3 and 4.3 mPa.s for AMC4 calculated for the first CS using the Urbain model [13]). The greater amount of a low viscous liquid formed during the slag attack to AMC2 predicted by the thermodynamic calculation agrees with the differential aspect of the corroded bar (Figure 1), as was described above. The simulation also explains the smaller difference in the wear between AMC3 and AMC4 evidenced under both the static and dynamic test conditions and by the slightly higher impurity level of AMC3 (especially the Fe_2O_3 content) which requires one additional CS to reach equilibrium (Table III).

Since the refractory bar encounters the liquid slag after the maximum temperature is reached, the materials undergo several transformations beforehand; the main processes include chemical reactions and physical changes such as binder pyrolysis, carbon oxidation (although minimal, it may occur to some degree), spinel formation, the carbothermal reduction of magnesia, and the porosity alteration accompanying most of them. In this sense, AMC2 is the refractory most sensitive to oxidation, and it exhibited the greatest PLC (Table I), even when the increase in spinel formation was similar to that of AMC3 [10]; the latter had a

notably small PLC, almost constant at approximately 0.25 % along five heating-cooling cycles up to 1400°C, which has been discussed previously by the authors [10]. On the other hand, AMC4 has a higher oxidation resistance (Table I), and the spinel forms slower (due to the granulometry of the periclase [11]). Therefore, although an increase in the open porosity was observed in the three AMC refractories when temperatures reached 1400°C, AMC3 retained the smallest apparent porosity values, as reported in previous works by the authors [10]. At the other extreme, AMC2 always exhibited the highest volume of open pores [10]. This is another factor that helped make AMC2 more sensitive to the slag attack. In turn, the low permeability of AMC3, which probably became below that of AMC2 and AMC4 with increasing temperature, was considered the main reason for the lower amount of slag penetration observed in SEM images of the corroded bar.

That said, another aspect of the slag corrosion behavior of the studied AMC refractories must be mentioned. The increase in wear during the rotary dipping test was different for the three refractories when compared to the cup test: 1.4, 1.9, and 2.8 times greater for AMC2, AMC3, and AMC4, respectively. Furthermore, the relative increase in wear for the bricks is in the reverse order of their inherent slag resistance. On one hand, the wear experienced by the AMC2 tested under dynamic conditions could be still underestimated despite the better method used to determine this parameter. Compared to its original dimensions, the expansion of the bar section of AMC2 is visible to the naked eye, which may be a consequence of permanent dimensional expansion due to several thermally activated transformations during the heating process (higher than the other two bricks), and extended slag penetration. Unfortunately, there is no way to consider the specific contribution of such a process in the final area of the corroded bar. However, it is important to be aware of the errors associated with the quantitative parameter obtained from this test, especially when it is used to rank different materials.

On the other hand, some characteristics of the AMC3 and AMC4 materials could have a negative impact under the rotary dipping test conditions and thus increase the difference in wear produced during the cup test. During this test, the liquid slag moves relatively to the refractory sample; for this reason, the material loss can be produced by erosion. Those particles roughly between 100 and 1000 μm in size are considered the most affected by this process [3, 4]; smaller particles were dissolved completely, and the larger particles resisted better to be dragged. The contribution of different particle size ranges for the three AMC bricks (calculated from the cumulative granulometric curves obtained by an *ad-hoc* methodology designed for this type of refractory [11]) is indicated in Table IV.

In this sense, AMC4 is the refractory with the highest contribution of particles that easily pull away from the material and the lowest amount of the most resistant particles. Moreover, even though it has more fine particles, the amount of spinel formed during heating which contributed to
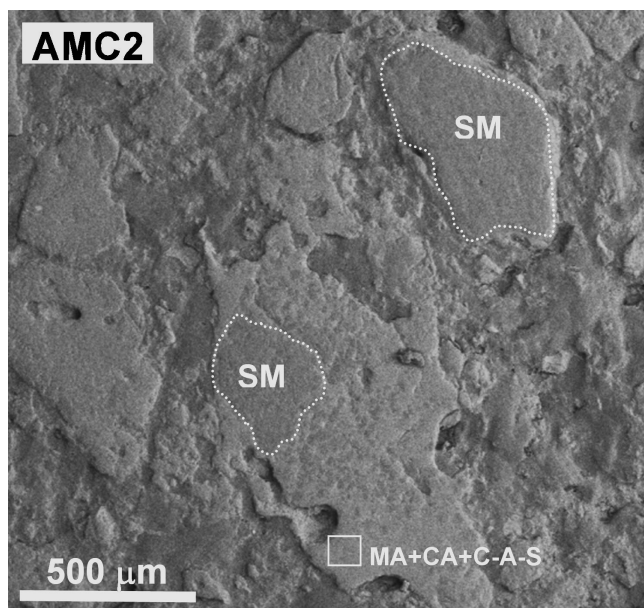

Figure 4. Sintered magnesia (SM) corroded particles in AMC2.

Table IV. Contribution of different particle size ranges for AMC bricks.

	AMC2 (wt.%)	AMC3 (wt.%)	AMC4 (wt.%)
> 1190$^{(1)}$ μm*	46	49	40
1190-105$^{(2)}$ μm**	49	47	54
< 105 μm	5	4	6

*Mesh # 16**Mesh # 140

stopping corrosion [2], is lower than in AMC2 and AMC3. Furthermore, periclase particles which did not react during the heating step, since they had less resistance than alumina particles [2, 3], encountered the slag, thus contributing to an increase in material loss due to corrosion. These aspects make AMC4 more sensitive to slag corrosion under dynamic conditions.

In the case of AMC3, the lower quality of the alumina particles, especially that of bauxite [2, 14, 15], is considered the key factor that sensitizes this brick under dynamic conditions. Bauxite particles were not identified in the interface with the slag in the corroded sample due to the high degradation of this type of alumina. Due to its high content of TiO_2 and SiO_2, the rapid incorporation of these ions into the slag by the erosion, attack, and dissolution of such particles, made the liquid more aggressive to the refractory [15]. The low permeability and small PLC of this AMC refractory surely counterbalanced the intrinsically low corrosion resistance of its main components.

CONCLUSIONS

Three different AMC bricks for steelmaking use were tested under different slag-refractory conditions, particularly in terms of the relative movement between them. In this work, the results of the testing under dynamic conditions (rotary dipping test) are reported and compared to those obtained under static conditions (cup test), The results and the analysis reported in this paper show how the evaluation of different refractories under different testing conditions helps create better comprehension from both points of view, i.e., the material's behavior and the experimental approach. The main conclusions are the following: i) a method to quantify corrosion wear based on the cross area of the original and the corroded bar, which involves image analysis and the identification of the refractory material-residual slag boundary, turned out to be good alternative for obtaining a more reliable indicator of material corrosion; ii) severe damage was determined at the refractory/slag interface of every AMC brick evaluated using the rotary dipping test, in which strong corroded aggregates, a degraded matrix, and the infiltration of slag through the particles' grain boundaries were observed, although the same new phases as those proposed under static conditions (cup test) were identified (MA spinel, CA$_6$, CA$_2$, CA, C$_3$A/C$_{12}$A$_7$ and silicon containing phases); iii) the corrosion wear determined when relative movement between the refractory sample and the slag was present (rotary dipping test) was higher than that obtained under static conditions (cup test) for all of the AMC bricks,

but there was no indication of a change in the corrosion mechanism; iv) the AMC brick with the highest content of periclase and high open porosity—AMC2—was the least resistant to the basic slag attack at 1600°C under dynamic conditions, which was linked to a low oxidation resistance and a large PLC, even when its increase in sensitivity under dynamic refractory-slag conditions in comparison to the static conditions in the cup test was less than in the other two refractories, AMC3 and AMC4; and v) the smaller particle size in AMC4 and the lower corrosion resistance inherent to the bauxite particles in AMC3 were considered the determining factors behind the greater increase of the wear determined in the rotary dipping test with respect to the wear obtained in the cup test.

ACKNOWLEDGEMENTS

REFERENCES

[1] Muñoz V, Galliano PG, Brandaleze E, Tomba Martinez AG. Chemical wear of Al2O3–MgO–C bricks by air and basic slag. J Eur Ceram Soc. 2015;**35**:1621. doi:10.1016/j.jeurceramsoc.2014.11.024.

[2] Muñoz V, Camelli S, Tomba Martinez AG. Slag corrosion of alumina-magnesia-carbon refractory bricks: Experimental data and thermodynamic simulation. Ceram Int. 2017;**43**:4562. doi:10.1016/j.ceramint.2016.12.114.

[3] Calvo WA, Moliné MN, Camelli S, Tomba Martinez AG. Slag corrosion of alumina-magnesia-carbon refractory bricks by different approaches. Ceram Int. 2020;**46**:24495. doi:10.1016/j.ceramint.2020.06.236.

[4] Calvo WA, Dignani ML, Galliano PG, Brandaleze E, Tomba Martínez AG. Basic slag corrosion of alumina–magnesia–carbon refractory bricks containing Al and Si antioxidants. Int J Appl Ceram Technol. 2022;**19**:2331. doi:10.1111/ijac.14017.

[5] Calvo WA, Pena P, Tomba Martinez AG. Post-mortem analysis of alumina-magnesia-carbon refractory bricks used in steelmaking ladles. Ceram Int. 2019;**45**:185. doi:10.1016/j.ceramint.2018.09.150.

[6] Tabatabaie-Hedeshi SM, Bavand-Vandchali M,

Naghizadeh R. Characterization and post-mortem analysis of Al2O3-MgO-C refractories used in steelmaking ladle furnaces. Eng Failure Anal. 2020;**116**:104697. doi:10.1016/j.engfailanal.2020.104697.

[7] Reynaert C, Śnieżek E, Szczerba J. Evolution of Refractory Materials for Rotary Cement Kiln Sintering Zone. Ceram-Silik. 2020;**64**:1. doi:10.1007/s11148-017-0123-y.

[8] Akkurt S, Leigh HD. Book Review: Théorie Mathématique de l'Électricité, First Part. Amer Ceram Bull. 2003;**82**:32. doi:10.1090/s0002-9904-1926-04191-4.

[9] Li X, Zhu B, Wang T. Electromagnetic field effects on the formation of MgO dense layer in low carbon MgO C refractories. Ceram Int. 2012;**38**:2883. doi:10.1016/j.ceramint.2011.11.061.

[10] Muñoz V, Pena Castro MP, Tomba Martinez AG. Physical, chemical, and thermal characterization of alumina–magnesia–carbon refractories. Ceram Int. 2014;**40**:9133. doi:10.1016/j.ceramint.2014.01.128.

[11] Calvo WA, Ortega P, Velazco MJ, Muñoz V, Pena Castro P, Tomba Martinez AG. Characterization of alumina-magnesia-carbon refractory bricks containing aluminium and silicon. Ceram Int. 2018;**44**:8842. doi:10.1016/j.ceramint.2018.02.069.

[12] Wang D, Li X, Wang H, Mi Y, Jiang M, Zhang Y. Dissolution rate and mechanism of solid MgO particles in synthetic ladle slags. J Non-Cryst Solids. 2012;**358**:1196. doi:10.1016/j.jnoncrysol.2012.02.014.

[13] Urbain G, Ambier F, Deletter M, Anseau MR. Correspondence analysis for describing the morphology of powders. Application to a commercial alumina powder. Br Ceram Soc. 1981;**80**:139. doi:10.1016/0001-6160(83)90117-7.

[14] Okushima S, Sato T, Yamamoto K, Nakano Y. Sex Differences in the Susceptibility of Mice to Infection Induced by *Mycobacterium intracellulare*. Taikabutsu Overseas. 1990;**10**:142. doi:10.1164/ajrccm/142.2.430.

[15] Sarpoolaky H, Zhang S, Argent BB, Lee WE. Influence of Grain Phase on Slag Corrosion of Low☐Cement Castable Refractories. J Am Ceram Soc. 2001;**84**:426. doi:10.1111/j.1151-2916.2001.tb00672.x.